ChemPhysChem

Research Article
doi.org/10.1002/cphc.202100853

Chemistry Europe
European Chemical Societies Publishing

www.chemphyschem.org

Polysulfide Speciation and Migration in Catholyte Lithium–Sulfur Cells

Matthew Sadd,[a] Marco Agostini,[a] Shizhao Xiong,[a] and Aleksandar Matic*[a]

Semi-liquid catholyte Lithium–Sulfur (Li–S) cells have shown to be a promising path to realize high energy density energy storage devices. In general, Li–S cells rely on the conversion of elemental sulfur to soluble polysulfide species. In the case of catholyte cells, the active material is added through polysulfide species dissolved in the electrolyte. Herein, we use operando Raman spectroscopy to track the speciation and migration of polysulfides in the catholyte to shed light on the processes taking place. Combined with ex-situ surface and electrochemical analysis we show that the migration of polysulfides is central in order to maximize the performance in terms of capacity (active material utilization) as well as interphase stability on the Li-metal anode during cycling. More specifically we show that using a catholyte where the polysulfides have the dual roles of active material and conducting species, e.g. no traditional Li-salt (such as LiTFSI) is present, results in a higher mobility and faster migration of polysulfides. We also reveal how the formation of long chain polysulfides in the catholyte is delayed during charge as a result of rapid formation and migration of shorter chain species, beneficial for reaching higher capacities. However, the depletion of ionic species during the last stage of charge, due to the conversion to and precipitation of elemental sulfur on the cathode support, results in polarization of the cell before full conversion can be achieved.

Introduction

The use of new technologies for energy storage can mitigate increased greenhouse gas emissions by enabling the electrification of the transport sector, as well as stabilising intermittent renewable electricity sources, such as solar and wind, that rely on the use of grid storage systems.[1–3] Lithium-ion batteries (LIBs) are already part of this transformation,[4,5] however, they are rapidly reaching their theoretical limit in terms of energy density. It is now clear that large improvements beyond state-of-the-art technologies require the implementation of new battery chemistries and cell configurations. Additionally, the LIB technology has drawbacks in terms of sustainability, i.e. the use of high capacity cathodes requiring the application of scarce and toxic transition metals, e.g. cobalt,[6] which also brings high cost.[7]

The conversion based Lithium–Sulfur (Li–S) technology has the potential to overcome many of the limitations of Li-ion batteries, with a higher theoretical capacity of the active material (S), 1672 vs. 274 mAh g^{-1} for $LiCoO_2$,[8,9] low cost,[10] higher abundancy of raw materials, and a lower environmental impact.[11] Despite these clear advantages, and examples of Li–S outperforming state-of-the-art Li-ion cells,[12,13] the full potential of Li–S cells is still not being realised in practice, with high energy density (high loading) concepts typically reporting only 60–80% active material utilisation.[10,14,15] This shortcoming is directly linked to the electrochemical conversion mechanism with dissolution/precipitation reactions taking place during discharge and charge. The formation of polysulfide species soluble in the commonly used liquid electrolytes at start of discharge results in the migration of active material into the bulk electrolyte driven by the chemical gradient.[11,16] This can result in loss of active material due to side reactions at the Li-metal anode or by too slow back diffusion to the cathode as the electrochemical reaction proceeds. Thus, tracking polysulfide speciation and migration kinetics in the cell is a key to unravel which processes and parts of the electrochemical reaction scheme are limiting the capacity of the cell.

Polysulfide speciation and related conversion mechanisms in Li–S cells using traditional carbon composite cathodes and liquid electrolytes has been studied with a wide range of techniques, including X-ray Absorption[17] and Diffraction,[18,19] UV-vis Spectroscopy,[20,21] Electron Paramagnetic Resonance Spectroscopy[22] and Raman Spectroscopy.[18,19,23–27] These studies commonly combine the analytical techniques with cyclic voltammetry or galvanostatic cycling to observe speciation at different depths or states of discharge and charge. From these studies, insights into possible reaction pathways have been proposed for the conversion reaction of sulfur species.[27,28] Despite the differences in polysulfide species identified along various pathways, it is commonly accepted that there is a formation of highly soluble polysulfide species (Li_2S_n) upon conversion of elemental sulfur,[29,30] which can diffuse throughout the electrolyte volume, from the cathode, through the

[a] M. Sadd, Dr. M. Agostini, Dr. S. Xiong, Prof. A. Matic
Department of Physics
Chalmers University of Technology
41296 Göteborg, Sweden
E-mail: matic@chalmers.se

Supporting information for this article is available on the WWW under https://doi.org/10.1002/cphc.202100853

separator, and all the way to the anode.[26] Typically longer chain polysulfides are observed in the electrolyte at the start of discharge and as the conversion process proceeds shorter polysulfides will dominate. One can note that apart from the effect of electrochemical conversion short chain polysulfides can be formed as a result of disproportionation reactions.[27,31] In the final step the discharge end-product Li_2S is formed, which has a low solubility in commonly used liquid electrolytes,[8,32] thus typically precipitating on the cathode surface, inhibiting further conversion reactions by limiting access to the carbon surface.[33] In addition to being a signature of a specific reaction pathway the polysulfide speciation in the bulk electrolyte also provides insights into the kinetics of the system and how efficient the migration of polysulfides is from and to the cathode during cycling, which is a key to ensure high active materials utilization.

To mitigate the migration of active material from the cathode Li-polysulfides (Li_2S_n) have been deliberately added to the electrolyte, forming a catholyte.[34] This buffers dissolution of polysulfide species from the cathode,[35] and it has been shown to stabilise the Li-metal anode by changing the composition of the solid electrolyte interphase (SEI).[34] In addition, the polysulfides in the electrolyte can also participate in the electrochemical reaction,[36] acting as a liquid electrode, and thereby increasing the overall capacity of the cell.[12,37] Several reports have been taking the catholyte concept even further using a sulfur free highly porous carbon support on the cathode side and introducing the active material only through the catholyte, having a semi liquid cell concept, reaching high loading of active material.[38,39] The electrochemical mechanism in catholyte cells is essentially the same as in traditional Li–S cells but the concept relies on to an even larger degree on efficient migration of polysulfides in and out of the carbon cathode side, due to the high solubility in the electrolyte and the open carbon host structure, during cycling. Recently it has been shown that the Li_2S_n species in the catholyte can also play the role of a Li-salt, i.e. providing ion conduction, paving the way for the removal of fluorine containing salts from Li–S cells.[35,38,40] In this type of catholyte the number of charge carriers will change during cycling and the speciation of polysulfides in the catholyte will influence both the efficiency of the conversion reaction but also the overall transport of Li-ions between the electrodes. Despite there being many examples of *in situ* studies for traditional sulfur/carbon composite cathode Li–S cells, there are only a few studies on catholyte type cells.[41]

In this study, we report on an investigation of polysulfide speciation and migration in catholyte Li–S cells during cycling using *operando* Raman Spectroscopy. In particular we compare the behaviour of catholytes with and without the use of a traditional Li-salt to reveal how the behaviour changes when the Li_2S_n-species in the catholyte act as both a Li-salt and active material. The *operando* analysis is complemented by *ex situ* cycling and surface analysis of Li-anodes from coin cells after charge and discharge. We show how the composition of the catholyte directly promotes selected speciation and migration of polysulfides and how this can be linked to performance in terms of specific capacity as well as interphase stability on Li-metal.

Results and Discussion

Figure 1 reports the physical characterisation of the two catholytes, with and without the addition of a supporting Li-salt, used in this study. The base catholyte is formed by the dissolution of Li and Li_2S in the tetraethylene glycol dimethyl ether (TEGDME) at a composition that corresponds to 5 wt% of Li_2S_8 and 0.4 M of $LiNO_3$ to provide compatibility and interphase formation on the Li-metal anode. The conductivity of the base catholyte is around 10^{-3} S/cm and this increases considerably when a traditional Li-salt is added (here LiTFSI). At the same time the viscosity of the catholyte increases with the addition of Li-salt. This behaviour can be rationalised by the two competing effects of increasing the number of charge carriers

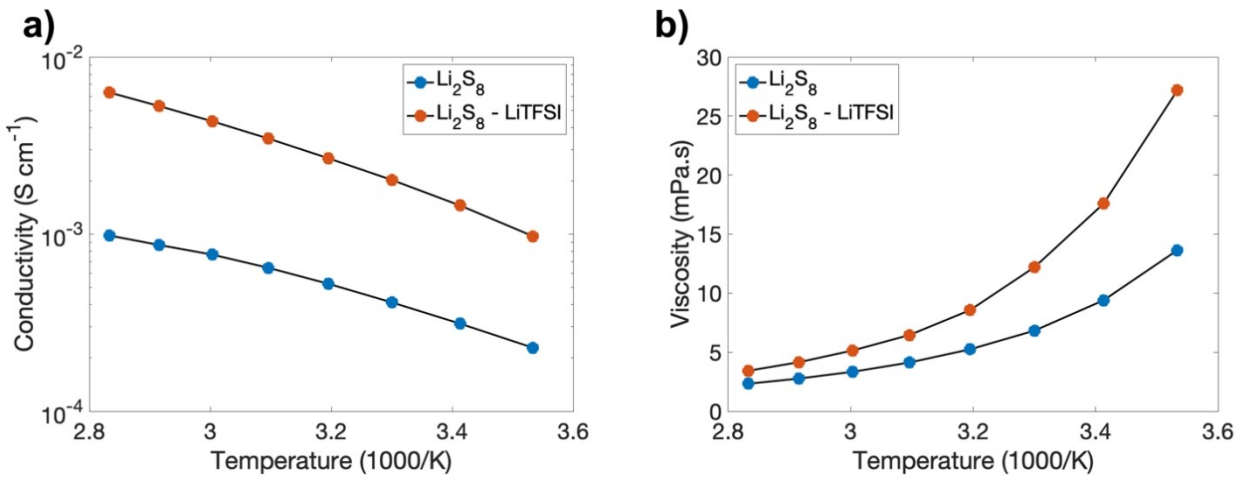

Figure 1. Physical characterisation of the two catholytes: 5 %wt Li_2S_8 in TEGDME + 0.4 M $LiNO_3$ without (blue) and with 0.5 M LiTFSI (orange). a) ionic conductivity and b) viscosity as function of the temperature.

and the increased ionic interaction after adding Li-salt. Thus, even though the conductivity of the catholyte with Li-salt is higher the mobility of the ions is expected to be lower which can have an impact on polysulfide migration.

Figure 2 shows the electrochemical characterization. Plating/stripping experiments were performed in symmetric Li/Li cells with the two catholytes and shown in Figure 2a. The results show that the overpotential rapidly stabilises over the first few cycles for both cells and no significant increase over 750 hours of continuous plating/stripping is observed. This highlights the compatibility of the catholytes with Li-metal from the combined effect of the addition of $LiNO_3$ in the catholyte formulation and the presence of polysulfides to form a stable interface.[34,42–44] The cell with the Li_2S_8–LiTFSI catholyte has a lower overpotential, overall lower cell resistance, which can be traced back to the improved ionic conductivity with the addition of LiTFSI. Figures 2b and 2c show galvanostatic voltage profiles from Li–S cells with the two catholytes and a sulfur free carbon working electrode as support for the electrochemical reactions, see experimental section in the Supporting Information. In the first cycle both cells only show a single step plateau at ~2 V, since the discharge starts with the reduction of long (nominally Li_2S_8) to short chain polysulfides, the sloping profile between 2.4 and 2 V, followed by the conversion of short chain

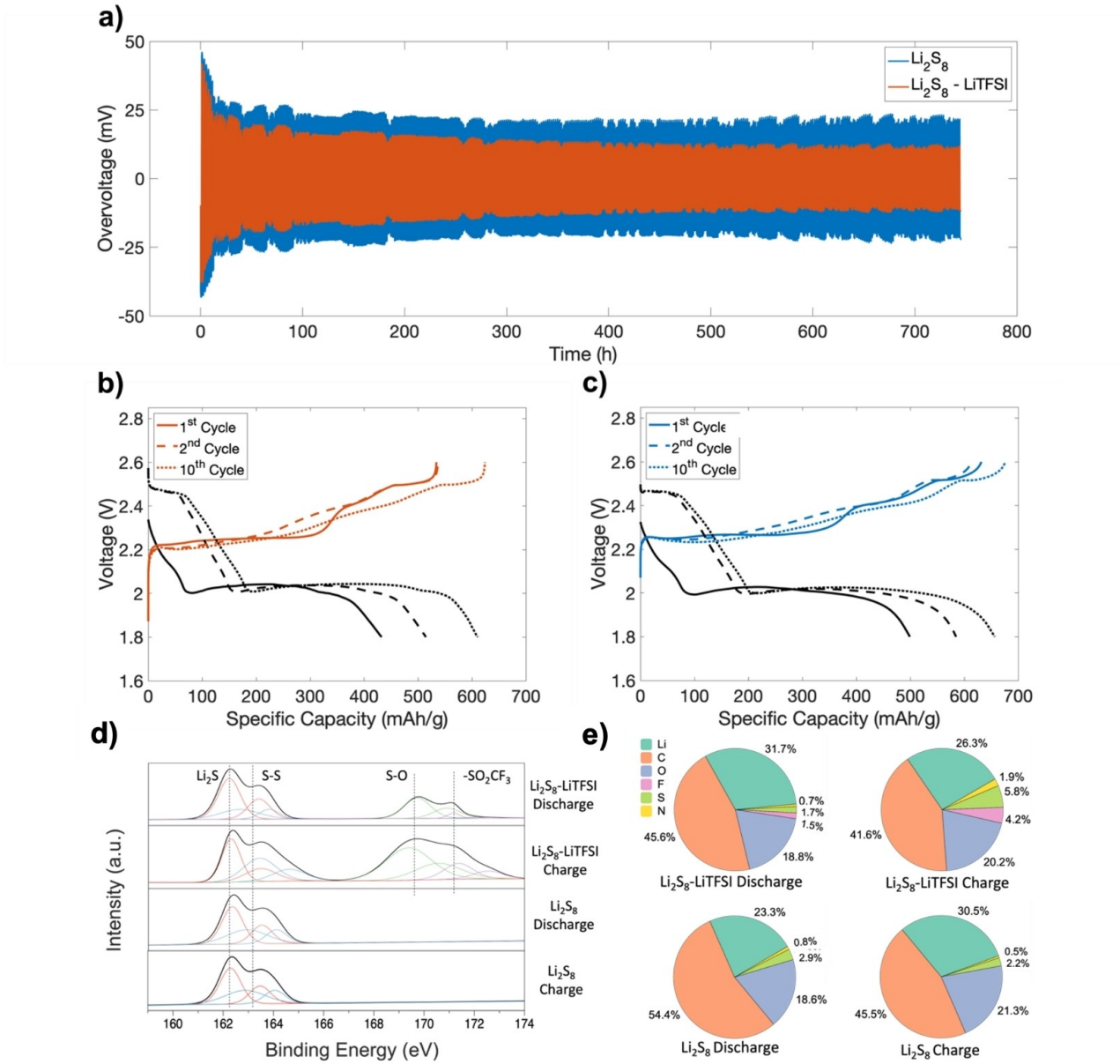

Figure 2. Electrochemical characterisation of Li–S cells using catholyte without (blue) and with 0.5 M LiTFSI (orange). a) Li plating/stripping experiment in symmetric Li/Li cells (0.1 mA/cm^2). Voltage profiles from galvanostatic cycling of the 1st, 2nd, and 10th cycles of the b) Li_2S_8–LiTFSI and c) Li_2S_8 catholyte coin cells (discharge/charge rate C/20). d) XPS spectra at the S 2p core level from Li-metal anodes retrieved from the coin cells. e) Elemental concentrations (at %), determined from XPS spectra, at the anode surface from Li_2S_8 and Li_2S_8–LiTFSI catholyte cells after charge and discharge.

polysulfides to Li_2S (2 V plateau). In the subsequent cycles the typical two voltage step profile is observed showing that full conversion to elemental sulfur, precipitating on the carbon working electrode, takes place during charge, in agreement with previous results on Li–S catholyte cells.[38]

The cell using the Li_2S_8 catholyte shows a higher discharge capacity compared to the cell with the Li_2S_8–LiTFSI catholyte (Figures 2b), i.e., the active material utilisation is higher in the cell without the traditional Li-salt. To efficiently use the active material in a catholyte cell, migration of polysulfides from the anode and the separator to the carbon cathode support is needed. As the reaction proceeds during discharge, a chemical gradient is created in the cell as polysulfides are converted to Li_2S and precipitated on the carbon support, driving the diffusion of polysulfides towards the cathode. As polysulfides reach the cathode and are reduced to Li_2S, which precipitates on the carbon surface and out of the electrolyte, Furthermore, the lower ion mobility in the Li_2S_8–LiTFSI catholyte will also slow down the diffusion of polysulfides. Thus, the migration of polysulfides will be faster in the Li_2S_8 catholyte leading to a higher active materials utilisation and increased capacity. Faster kinetics in the Li_2S_8 catholyte could influence the Li_2S deposition rate on the carbon electrode which could influence the morphology/porosity of the deposits. A more open structure formed at high deposition rates would allow the reaction to proceed further compared to a dense structure that efficiently blocks the access to the carbon support and limits further conversion reactions.[40]

Since a larger portion of polysulfides react at the carbon surface when the Li_2S_8 catholyte is used, it is expected that the concentration of polysulfides at the anode will be lower leading to less deposition of sulfide species on the Li-metal anode surface. To confirm this and to determine the composition of the passivation layer on the Li-metal anode with the two catholytes, X-ray photoelectron spectroscopy (XPS) was performed on Li-metal anodes retrieved from coin cells after full discharge and charge. The S2p core level spectra, Figure 2d and Table S1 (in the Supporting Information), show the sulfur-related species formed on the Li-metal surface. At the high binding energies, we find signatures of S–O and SO_2–CF_3 species on the surface of the anode from the Li_2S_8–LiTFSI catholyte cell, formed as a result of breakdown of the TFSI-anion. At lower binding energies signatures of Li_2S and S–S–O species are found in the spectra from the anodes cycled with both catholytes as consequence of the presence of Li_2S_n species in the catholyte. Comparing the intensity of the peaks in this region, we can note that the concentration of these species is larger in the case of the Li_2S_8–LiTFSI catholyte being used. In addition, the intensity of the peaks at higher binding energy also grows after charge, indicating a continuous breakdown of the TFSI-anion. Thus, the interphase formed in the presence of the Li_2S_8 catholyte is more stable. This is further underlined when considering the elemental compositions of the interphase layers on the anode surfaces, Figure 2e. When using the Li_2S_8–LiTFSI catholyte there is an increase in sulfur, fluorine, and nitrogen concentration between the first discharge and charge, a consequence of the breakdown of $TFSI^-$ and the deposition of Li_2S_n. In contrast, the cell using the Li_2S_8 catholyte has an elemental concentration at the anode surface that is the same after discharge and charge. Viewing the XPS results together with the plating/stripping data, this confirms that even without the presence of LiTFSI, the Li_2S_8-catholyte has the ability to build a stable SEI,[45] and that the fluctuation in the SEI composition during cycling, i.e. between charged and discharged states, is reduced.

To gain further insights into the electrochemical mechanism and polysulfides migration in the catholyte cells, *operando* confocal Raman spectroscopy was performed during galvanostatic discharge/charge, using a combined optical and electrochemical cell. The cell was designed to be as analogous to a coin cell, with the same electrode size and the same volume of catholyte added in the cell. The galvanostatic charge discharge voltage profiles from the *operando* cell, Figure S1, are in good agreement with the coin cell data and the two cells also show similar specific capacities. In the operando experiment, Raman spectra are collected from a small volume in the catholyte in close proximity to the anode surface, Figure 3a. From the spectra collected after assembling the cell, but before first discharge, Figure 3b, a strong Raman band is observed around 535 cm^{-1} which can be assigned to the S_3*− radical species[19,46,47] and two weaker bands are found at 372 cm^{-1} and 437 cm^{-1} originating from long chain polysulfide species, such as S_6^{2-} and S_8^{2-}.[23,47–50] Thus, already in the bare catholyte there is a distribution of polysulfide species as a result of disproportionation reactions.

To follow the change in speciation close to the anode Raman spectra were collected continuously during discharge and charge for cells with the two catholytes. After full discharge the intensity of signatures related to polysulfides is very low, Figure S2c, confirming that a large amount of Li_2S_n polysulfides have participated in the electrochemical reaction and been reduced to insoluble Li_2S that is deposited on the carbon cathode support. The same behaviour is expected during charge, since the polysulfides should be oxidised to S_8 and elemental sulfur should be deposited on the carbon cathode support. However, Raman bands corresponding to polysulfides can still be discerned after full charge, Figure S2d. Thus, total conversion of Li_2S_n to S_8 does not occur and polysulfide species remain in the electrolyte which can be due to a lack of electrolyte conductivity as the polysulfide speciation changes towards long chain polysulfides reducing the total ion concentration in the catholyte, and thereby the conductivity, leading to cell polarisation before all polysulfide species can be fully converted.

Using the Raman spectra to gain further insight, we quantify the evolution of the strong band related to S_3*− species (535 cm^{-1}) during cycling and the weaker bands related to long chain species S_6^{2-}/S_8^{2-} (372 $cm \cdot^1$ and 437 $cm \cdot^1$).[23,47] In Figures 3c and d the development of the intensities of the S_3*− and S_8^{2-} bands (535 cm^{-1} and 372 $cm \cdot^1$ respectively) are overlaid on the voltage profiles during the first cycle. During the first discharge step, 2.4–2.1 V, there is a rapid increase in the band corresponding to the S_3*− species and sharp decrease in the intensity of the band related to long chain polysulfides. This is

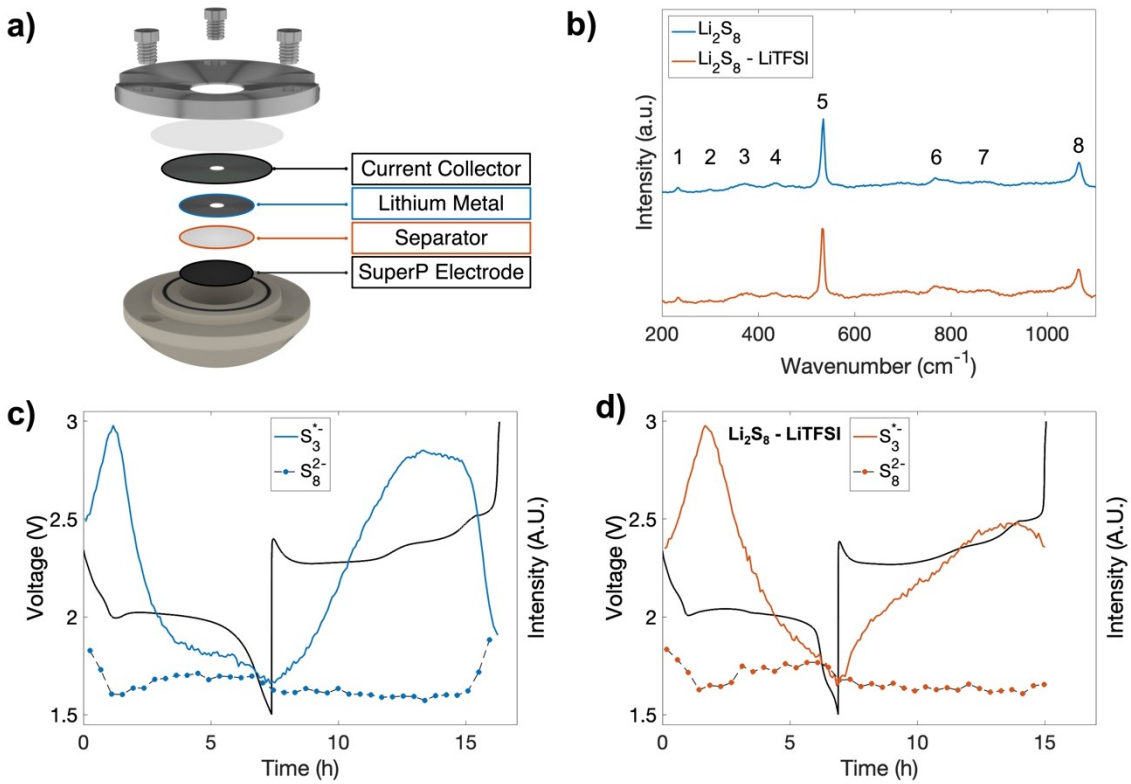

Figure 3. Raman spectra from the operando cell and polysulfide speciation during discharge and charge. a) Cell configuration for operando Raman experiments. The spectra are taken in the bulk catholyte close to the Li-metal anode. b) Raman spectra obtained from the Li_2S_8 (blue) and Li_2S_8–LiTFSI (orange) catholytes in the operando cell, band assignment in Table S2. Intensity of the S_3^{*-} Raman band (535 cm^{-1}) and long chain polysulfide band (372 cm^{-1}) overlaid on the galvanostatic voltage profiles when cycling with the c) Li_2S_8 and d) Li_2S_8–LiTFSI catholytes.

the region where we expect the conversion of long chain polysulfides to shorter polysulfides to take place and the behaviour of the Raman intensities thus confirms this process. At the start of the voltage plateau at 2.1 V the intensity of the 535 cm^{-1} band rapidly drops in the Li_2S_8 catholyte, Figure 3c. This result is consistent with a mechanism where there is a rapid migration of polysulfide species to the cathode from the anode, where the Raman spectra are taken, as Li_2S is formed and precipitated on the cathode support. In the case of the Li_2S_8–TFSI catholyte, the decrease in intensity of the 535 cm^{-1} band is much slower and continues during almost the whole discharge, Figure 3d, in agreement with a slower migration of polysulfide species.

At the start of the 1st charge, the concentration of S_3^{*-} increases slowly, but continuously, in the cell with the Li_2S_8 catholyte and reaches a maximum at 60% into the charge process, whereas the concentration of longer chain polysulfides remains low until the very last part of the charge process, Figure 3c. To rationalise this behaviour, we can envisage a reaction path where in the initial stages of charge only short chain polysulfides are created, up to Li_2S_4, and the longer species are not formed until later into the charge process. In fact, the onset of the constant intensity of the S_3^{*-} Raman band coincides with a kink in the voltage profile which could indicate the formation of S_6^{2-}, which can disproportionate to form the observed S_3^{*-} species. As the concentration of S_3^{*-} species decrease there is again a kink in the voltage profile and also an increase in the signal corresponding to S_8^{2-} species. In the Raman spectra of the Li_2S_8–TFSI catholyte, the S_3^{*-} Raman band intensity increases more gradually at the start of charge, Figure 3d, pointing to a mechanism where conversion is slower. Furthermore, in the Li_2S_8–TFSI catholyte the presence of a band at 372 cm^{-1} is not detected at the end of the 1st charge and the decrease of the S_3^{*-} band intensity is small. This can be rationalised by the fact that polysulfide mobility is lower due to the higher viscosity and that the observation of the formed species on the anode side is delayed.

In Figure 4, the evolution of the Raman band intensities across multiple cycles is shown. In the Li_2S_8 catholyte, the S_3^{*-} band intensity reaches 90% of the maximum value during the first discharge. In each subsequent cycle the intensity of this band remains high, but with a small decrease in each cycle. For the Li_2S_8–LiTFSI catholyte, the S_3^{*-} bands intensity reaches 65% at charge compared to discharge, but then remains rather stable. This suggests that in the Li_2S_8–LiTFSI catholyte sulfur species are irreversibly consumed in the first cycle, consistent with the finding of a higher sulfur content of the SEI formed on the Li-metal anode in the Li_2S_8–LiTFSI catholyte system. Such consumption is observed to be less significant in the Li_2S_8 catholyte.

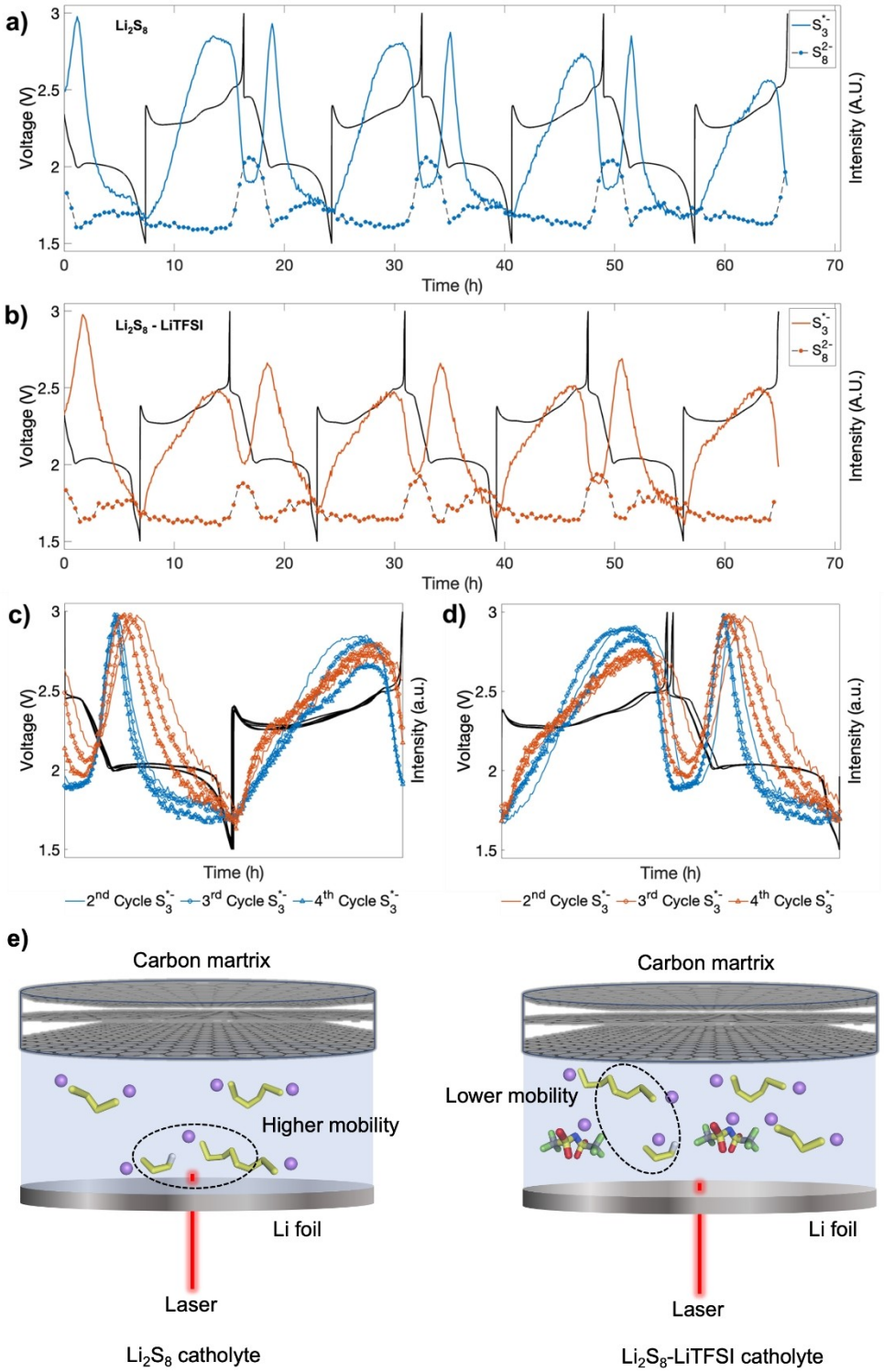

Figure 4. Evolution of Raman band intensities of catholyte Li–S cells during multiple cycles. Intensity of 372 cm^{-1} (S_8^{2-}) and 535 cm^{-1} (S_3*—) bands and voltage profiles over 4 cycles for the a) Li_2S_8 catholyte (blue) and b) Li_2S_8—LiTFSI catholyte (orange). Intensities of the S_3*— band and voltage profiles of each cycle overlaid and normalised to the maximum discharge and charge times for the Li_2S_8 catholyte (blue) and Li_2S_8—LiTFSI catholyte (orange) with c) a discharge/charge alternance and d) a charge/discharge alternance, voltage profiles shown in Figure S3. e) Schematic of polysulfide mobility in different catholytes.

In the Li_2S_8 catholyte the Raman band corresponding to long chain polysulfides increases during the final stages of the 1st charge and reaches a maximum during the 2.4 V plateau of the 2nd discharge, thus there is a delay in the observation of the

species at the anode side compared to their formation in the cathode. In the case of the Li_2S_8–LiTFSI catholyte the maximum of S_8^{2-} Raman band occurs little bit later, close to the end of the first plateau during discharge, in agreement with the previous discussion on a lower mobility of the polysulfide species. It should be noted that for both systems only the maxima seen during the 2.4 V plateau are considered as significant for the S_8^{2-} Raman as the absolute intensity of this band is rather low. Increases in intensity at other points during discharge and charge can be a result of the baselining of data with a significant fluorescent background.

To gain further insight into the role of polysulfide species on cell performance, the evolution of the intensity of the S_3*− band intensity and the corresponding voltage profiles are overlaid and normalised to the charge/discharge times to allow a direct comparison of the behaviour of the two cells across multiple cycles (Figures 4 c and d). For the Li_2S_8 catholyte, (Figure 4c), the S_3*− band intensity maximum seen during discharge for the 2nd, 3rd, and 4th cycles appears at the same depth of discharge and the intensity increase starts at the same depth of discharge. However, for the Li_2S_8–LiTFSI catholyte, the intensity maxima are observed progressively earlier in the discharge. Figure 4d shows the same analysis, but with a charge/discharge alternance. In Figure 4d, for the Li_2S_8 catholyte it can be seen that there is a minimum in the S_3*− band intensity as the cell reaches full charge, and this minimum remains during the 2.4 V plateau in the discharge. However, for the Li_2S_8–LiTFSI catholyte, this minimum is not observed during charge but only after the 2.4 V plateau in the subsequent discharge. With each subsequent cycle this minimum is observed closer to the cell's charged state.

This delay in the positions of both the minima and maxima seen in the Li_2S_8–LiTFSI catholyte, and their subsequent shift, suggests that polysulfide mobility in the electrolyte changes with each cycle. It must be noted that the Raman spectra were measured close to the anode, thus the measured intensities of polysulfide species reflect the concentration of species that have been converted at the cathode and migrated to the anode. Thus, the difference in the position of the minima and maxima of between the two catholytes directly reflects the migration of polysulfides (Figure 4e). The shift of the maxima and minima for the Li_2S_8–LiTFSI catholyte with each cycle, can be related to that polysulfide species and the Li-salt in the catholyte are consumed during cycling, reducing the electrolyte viscosity, and increasing the mobility of remaining species.

To evaluate the impact of polysulfides migration on long-term cycling of Li–S cells using catholytes, coin cells with Li_2S_8–LiTFSI and Li_2S_8 catholytes were cycled and their cycling performance is shown in Figure S4. The coin cells deliver a specific capacity of 538 mAh g^{-1} and 559 mAh g^{-1} after 60 cycles for Li_2S_8–LiTFSI and Li_2S_8 catholytes, respectively. This indicates that stable cycling of Li–S cell can be realized even with considerable migration of polysulfides in the catholyte. It further underlines that a stable SEI on Li, as discussed in Figure 2, plays a key role on suppressing shuttle effect and utilization of active mass in Li–S cells with catholyte configuration.

Conclusions

We report an insight into the mechanism and migration of polysulfides during discharge and charge in catholyte Li–S cells using operando Raman spectroscopy. We show that using a catholyte only based on the addition of polysulfides (e.g., no traditional Li-salt, such as LiTFSI, is present) results in a higher mobility of polysulfide species and faster migration in the cell, which is beneficial for active material utilisation. The mechanism behind this behaviour originates from a faster diffusion of short chain polysulfide species and affects the subsequent conversion of these species. The removal of a traditional Li-salt also improves the stability of the SEI formed on the Li-metal anode.

Acknowledgments

M.S and A.M. acknowledge the support from the Swedish Energy Agency through the STARC project.

Conflict of Interest

The authors declare no conflict of interest.

Data Availability Statement

The data that support the findings of this study are available from the corresponding author upon reasonable request.

Keywords: lithium–sulfur (Li–S) battery · operando Raman spectroscopy · catholyte · polysulfides · radical species

[1] H. Zhao, Q. Wu, S. Hu, H. Xu, C. N. Rasmussen, *Appl. Energy* **2015**, *137*, 545–553.
[2] S. Chu, A. Majumdar, *Nature* **2012**, *488*, 294–303.
[3] S. Chu, Y. Cui, N. Liu, *Nat. Mater.* **2016**, *16*, 16–22.
[4] J. B. Goodenough, K. S. Park, *J. Am. Chem. Soc.* **2013**, *135*, 1167–1176.
[5] M. Li, J. Lu, Z. Chen, K. Amine, *Adv. Mater.* **2018**, *30*, 1–24.
[6] B. Swain, *Sep. Purif. Technol.* **2017**, *172*, 388–403.
[7] S. Hess, M. Wohlfahrt-Mehrens, M. Wachtler, *J. Electrochem. Soc.* **2015**, *162*, A3084–A3097.
[8] S. S. Zhang, *J. Power Sources* **2013**, *231*, 153–162.
[9] N. Nitta, F. Wu, J. T. Lee, G. Yushin, *Mater. Today* **2015**, *18*, 252–264.
[10] S. H. Chung, A. Manthiram, *Adv. Mater.* **2019**, *31*, 39–42.
[11] X. Ji, L. F. Nazar, *J. Mater. Chem.* **2010**, *20*, 9821–9826.
[12] M. Agostini, J. Y. Hwang, H. M. Kim, P. Bruni, S. Brutti, F. Croce, A. Matic, Y. K. Sun, *Adv. Energy Mater.* **2018**, *8*, 1–7.
[13] S. Nanda, A. Bhargav, A. Manthiram, *Joule* **2020**, *4*, 1121–1135.
[14] R. Kumar, J. Liu, J. Y. Hwang, Y. K. Sun, *J. Mater. Chem. A* **2018**, *6*, 11582–11605.
[15] U. Košir, I. K. Cigić, J. Markelj, S. D. Talian, R. Dominko, *Electrochim. Acta* **2020**, *363*, DOI 10.1016/j.electacta.2020.137227.
[16] A. Fotouhi, D. J. Auger, K. Propp, S. Longo, M. Wild, *Renewable Sustainable Energy Rev.* **2016**, *56*, 1008–1021.
[17] M. Cuisinier, P. E. Cabelguen, S. Evers, G. He, M. Kolbeck, A. Garsuch, T. Bolin, M. Balasubramanian, L. F. Nazar, *J. Phys. Chem. Lett.* **2013**, *4*, 3227–3232.

[18] W. Zhu, A. Paolella, C. S. Kim, D. Liu, Z. Feng, C. Gagnon, J. Trottier, A. Vijh, A. Guerfi, A. Mauger, C. M. Julien, M. Armand, K. Zaghib, *Sustain. Energy Fuels* **2017**, *1*, 737–747.
[19] J.-T. Yeon, J.-Y. Jang, J.-G. Han, J. Cho, K. T. Lee, N.-S. Choi, *J. Electrochem. Soc.* **2012**, *159*, A1308–A1314.
[20] M. U. M. Patel, R. Demir-Cakan, M. Morcrette, J. M. Tarascon, M. Gaberscek, R. Dominko, *ChemSusChem* **2013**, *6*, 1177–1181.
[21] H. Marceau, C. S. Kim, A. Paolella, S. Ladouceur, M. Lagacé, M. Chaker, A. Vijh, A. Guerfi, C. M. Julien, A. Mauger, M. Armand, P. Hovington, K. Zaghib, *J. Power Sources* **2016**, *319*, 247–254.
[22] Q. Wang, J. Zheng, E. Walter, H. Pan, D. Lv, P. Zuo, H. Chen, Z. D. Deng, B. Y. Liaw, X. Yu, X. Yang, J.-G. Zhang, J. Liu, J. Xiao, *J. Electrochem. Soc.* **2015**, *162*, A474–A478.
[23] J. Hannauer, J. Scheers, J. Fullenwarth, B. Fraisse, L. Stievano, P. Johansson, *ChemPhysChem* **2015**, *16*, 2755–2759.
[24] M. Agostini, D. H. Lim, M. Sadd, C. Fasciani, M. A. Navarra, S. Panero, S. Brutti, A. Matic, B. Scrosati, *ChemSusChem* **2017**, *10*, 3490–3496.
[25] H. L. Wu, L. A. Huff, A. A. Gewirth, *ACS Appl. Mater. Interfaces* **2015**, *7*, 1709–1719.
[26] R. Bouchal, A. Boulaoued, P. Johansson, *Batteries & Supercaps* **2020**, *3*, 397–401; Supercaps **2020**, 3, 397–401.
[27] M. Wild, L. O'Neill, T. Zhang, R. Purkayastha, G. Minton, M. Marinescu, G. J. Offer, *Energy Environ. Sci.* **2015**, *8*, 3477–3494.
[28] D. Zheng, X. Zhang, J. Wang, D. Qu, X. Yang, D. Qu, *J. Power Sources* **2016**, *301*, 312–316.
[29] G. Li, S. Wang, Y. Zhang, M. Li, Z. Chen, J. Lu, *Adv. Mater.* **2018**, *30*, 1–19.
[30] J. Scheers, S. Fantini, P. Johansson, *J. Power Sources* **2014**, *255*, 204–218.
[31] H. Shin, M. Baek, A. Gupta, K. Char, A. Manthiram, J. W. Choi, *Adv. Energy Mater.* **2020**, *10*, 1–21.
[32] Y. Liu, Y. Pan, J. Ban, T. Li, X. Jiao, X. Hong, K. Xie, J. Song, A. Matic, S. Xiong, *Energy Storage Mater.* **2020**, *25*, 131–136.
[33] S. Drvarič Talian, G. Kapun, J. Moškon, A. Vizintin, A. Randon-Vitanova, R. Dominko, M. Gaberšček, *Chem. Mater.* **2019**, *31*, 9012–9023.
[34] M. Agostini, S. Xiong, A. Matic, J. Hassoun, *Chem. Mater.* **2015**, *27*, 4604–4611.
[35] M. Agostini, D. H. Lim, M. Sadd, J. Y. Hwang, S. Brutti, J. W. Heo, J. H. Ahn, Y. K. Sun, A. Matic, *ChemSusChem* **2018**, *11*, 2981–2986.
[36] Y. Yang, G. Zheng, Y. Cui, *Energy Environ. Sci.* **2013**, *6*, 1552–1558.
[37] C. Cavallo, M. Agostini, J. P. Genders, M. E. Abdelhamid, A. Matic, *J. Power Sources* **2019**, *416*, 111–117.
[38] D. H. Lim, M. Agostini, F. Nitze, J. Manuel, J. H. Ahn, A. Matic, *Sci. Rep.* **2017**, *7*, 1–9.
[39] S. H. Chung, A. Manthiram, *Adv. Mater.* **2018**, *30*, 1–9.
[40] R. Xu, I. Belharouak, J. C. M. Li, X. Zhang, I. Bloom, J. Bareño, *Adv. Energy Mater.* **2013**, *3*, 833–838.
[41] Y. Zhang, C. Fincher, S. McProuty, M. Pharr, *J. Power Sources* **2019**, *434*, 226727.
[42] M. J. Lacey, A. Yalamanchili, J. Maibach, C. Tengstedt, K. Edström, D. Brandell, *RSC Adv.* **2016**, *6*, 3632–3641.
[43] S. Xiong, K. Xie, Y. Diao, X. Hong, *J. Power Sources* **2014**, *246*, 840–845.
[44] S. Xiong, K. Xie, Y. Diao, X. Hong, *Electrochim. Acta* **2012**, *83*, 78–86.
[45] S. Xiong, K. Xie, Y. Diao, X. Hong, *J. Power Sources* **2013**, *236*, 181–187.
[46] T. Chivers, P. J. W. Elder, *Chem. Soc. Rev.* **2013**, *42*, 5996–6005.
[47] M. Hagen, P. Schiffels, M. Hammer, S. Dörfler, J. Tübke, M. J. Hoffmann, H. Althues, S. Kaskel, *J. Electrochem. Soc.* **2013**, *160*, A1205–A1214.
[48] O. El Jaroudi, E. Picquenard, A. Demortier, J. P. Lelieur, J. Corset, *Inorg. Chem.* **1999**, *38*, 2394–2401.
[49] G. J. Janz, E. Roduner, J. W. Coutts, J. R. Downey, *Inorg. Chem.* **1976**, *15*, 1751–1754.
[50] F. P. Daly, C. W. Brown, *J. Phys. Chem.* **1975**, *79*, 350–354.

Manuscript received: December 1, 2021
Revised manuscript received: December 23, 2021
Accepted manuscript online: December 23, 2021
Version of record online: January 12, 2022